Planetary and Space Science 89 (2013) 15–20

Contents lists available at ScienceDirect

Planetary and Space Science

journal homepage: www.elsevier.com/locate/pss

Redistribution of lunar polar water to mid-latitudes and its role in forming an OH veneer

W.M. Farrell [a,e,*], D.M. Hurley [b,e], R.R. Hodges [c,e], R.M. Killen [a,e], J.S. Halekas [d,e], M.I. Zimmerman [a,e,f], G.T. Delory [d,e]

[a] NASA/Goddard SFC, Greenbelt, MD, United States
[b] Johns Hopkins/Applied Physics Laboratory, Laurel, MD, United States
[c] University of Colorado, Boulder, CO, United States
[d] University of California, Berkeley, CA, United States
[e] NASA Lunar Science Institute, Moffett Field, CA, United States
[f] Oak Ridge Associated Universities, Oak Ridge, TN 050813, United States

ARTICLE INFO

Article history:
Received 3 October 2012
Received in revised form
8 May 2013
Accepted 16 May 2013
Available online 3 June 2013

Keywords:
Moon
Lunar poles
Sputtering
Impact vaporization
Desorption
Transport

ABSTRACT

We suggest that energization processes like ion sputtering and impact vaporization can eject/release polar water molecules residing within cold trapped regions with sufficient velocity to allow their redistribution to mid-latitudes. We consider the possibility that these polar-ejected molecules can contribution to the water/OH veneer observed as a 3 μm IR absorption feature at mid-latitudes by Chandrayaan-1, Cassini, and EPOXI. We find this source cannot fully account for the observed IR feature, but could be a low intensity additional source.

Published by Elsevier Ltd.

1. Introduction

Chandrayaan-1's M-cubed instrument discovered the presence of surficial OH and water veneer on the Moon (via the 2.8–3 μm IR absorption feature) that progressively intensified from ~60–70° latitude to extreme poleward locations in both the northern and southern hemispheres (Pieters et al., 2009; McCord et al., 2011). A similar signature was also detected in IR instruments onboard Deep Impact and Cassini (Sunshine et al., 2009; Clark et al., 2009), and all three observational sets were reported simultaneously in late 2009, presenting a convincing cross-correlated case for the water veneer. A number of ideas have been put forth to account for the surficial water, including manufacturing of water via the solar wind and possibly the presence of water in nominally anhydrous mineralogy (Housley et al., 1974; Pieters et al., 2009; Dyar et al., 2010; McCord et al., 2011). However, the source of the mid-latitude water and OH veneer is still unknown.

In contrast, some of the sunlight-sheltered cold polar craters are confirmed to have accumulations of water. Recent LCROSS findings (Colaprete et al., 2010; Schultz et al., 2010) suggest that Cabeus crater contains large amounts of water ice (~5–10% by weight). However, Lunar Reconnaissance Orbiter neutron spectrometry indicates that not every substantial polar crater appears to have significant H-bearing mineralogy (Mitrofanov et al., 2010). FUV albedo also suggests that surficial water frost may also be present in some of the polar craters (Gladstone et al., 2012). Any polar icy regolith is exposed to harsh space environment that includes micro-meteoroid impacts and solar wind sputtering; processes that can energize and transport molecules in an extended region about the pole.

Given the proximity of the known polar water source to the locations of the mid-latitude veneer, an obvious question is whether the icy regolith regions within polar craters can be a source for the thin water/OH veneer at lower latitudes (~70–85°); polar crater water being released by space environmental erosion processes (impact vaporization, sputtering, etc.). In essence, we revisit the idea that lunar ices are eroded (Arnold, 1979; Lanzerotti et al., 1981) to contribute to the exosphere (Morgan and Shemansky, 1991) and adjacent surface. We thus will test the

* Corresponding author at: NASA/Goddard SFC, Greenbelt, MD, United States. Tel.: +1 301 286 4446; fax: +1 301 286 1683.
E-mail address: william.m.farrell@nasa.gov (W.M. Farrell).

0032-0633/$ - see front matter Published by Elsevier Ltd.
http://dx.doi.org/10.1016/j.pss.2013.05.009

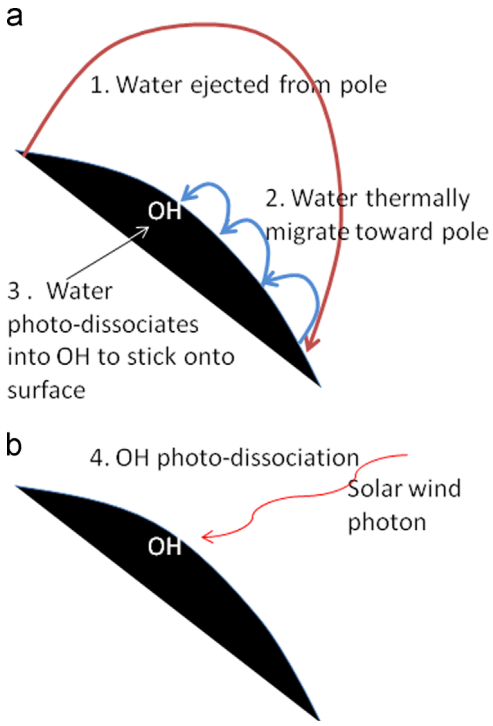

Fig. 1. An illustration of the process in creating the OH and water veneer.

hypothesis that regions containing icy-regolith at the poles are a water 'fountain' source ejecting water molecules over an extended latitude range.

Fig. 1 illustrates the concept. In the polar region, environmental processes like impact vaporization and sputtering release water molecules from the cold trap. The water molecules have sufficient kinetic energy to be transported to mid-latitudes, where they land on a warm surface and thus have a very short residency time. They undergo thermal migration back toward the pole in ballistic 'hopping' trajectories, as illustrated in Fig. 1a (Crider and Vondrak, 2000). However, the photo-dissociation time for water is less than the polar migration time and thus over 90% of these molecules should be destroyed before their migration to the pole is complete (Crider and Vondrak, 2000). The resulting photo-dissociated product OH then resides or 'sticks' on the surface for an extended period due to its high desorption temperature of $>400\ ^{\circ}$K (Hibbitts et al., 2011). We thus have the creation of a longer-lived OH surface veneer in tandem with an active water transport cycle. In this concept, we are not creating water, but only considering the redistribution of pre-existing water from the poles to a more extended region in latitude.

2. Models of the lunar polar icy-regolith

Based on the LCROSS (Colaprete et al., 2010; Schultz et al., 2010), Lunar Prospector Neutron Spectrometer (Feldman et al., 1998), and the evolving LRO/LEND observations (Mitrofanov et al., 2010), water molecules are located in the near-surface of some of the permanently shadowed regions at the poles. Mitrofanov et al. (2010) reported that south polar craters Shoemaker and Cabeus have a statistically significant neutron suppression associated with H-bearing minerals. They also reported that neutron suppressed regions may even extend beyond the shadowed crater regions to topside surface.

We present two possible models of the icy regolith within polar craters. As we demonstrate, results from these models can be scaled for other possible icy-regolith concentrations and configurations. Models 1 considers that the polar craters have a surficial exposed icy-regolith with a mixed ice content at 0.1 wt% fraction. The total area of this exposed surficial ice is assumed to be $A_s \sim 10^{10}$ m^2. This area is consistent with the floor of Cabeus and Shoemaker craters in south pole. Model 2 assumes a case where a 5 wt% icy-regolith layer is present in these same craters, but now buried at a depth of 3 cm, at 20 cm, and 50-cm. Comparison of fast and epithermal neutron levels suggest the presence of a water-free/dry top layer over buried icy regolith; this layer being possibly of 10's of centimeters in thickness (Feldman et al., 1998).

3. Model 1: energization processes and water release at the crater floor

We consider four processes that have the ability to remove water molecules from an icy-regolith: solar wind ion sputtering, electron stimulated desorption (ESD), photon stimulated desorption (PSD) and impact vaporization. All four apply to Model 1 but only the last, impact vaporization, applies to Model 2.

3.1. Sputtering

For surface-incident solar wind ions, the sputtering yield for a 1 keV proton on an ice-substrate is near 0.5 molecules per ions (Johnson, 1990). We now consider the yield for ice mixed with regolith at 0.1%. We apply equation 3.22 of Johnson (1990) to derive a weighted sputtering yield for such a mixture, which is $Y \sim 10^{-3}$ water molecules per incident solar wind ion. The nominal solar wind ion flux incident at the exposed surface above 85° latitude is $<2\times10^{11}$/m^2-s. However, the situation is more complicated for ion inflow into sheltered polar craters like Shoemaker (Farrell et al., 2010; Jackson et al., 2011; Zimmerman et al., 2011). Plasma models suggest that the near-horizontally flowing solar wind ions eventually get diverted into larger polar craters (10's of km in diameter) via plasma ambipolar E-fields. However, the instantaneous ion inflow varies as a function of location within a crater (Farrell et al., 2010; Jackson et al., 2011). Defining the ratio of ion flux to nominal solar wind ion flux as F/F_{sw}, this ratio is

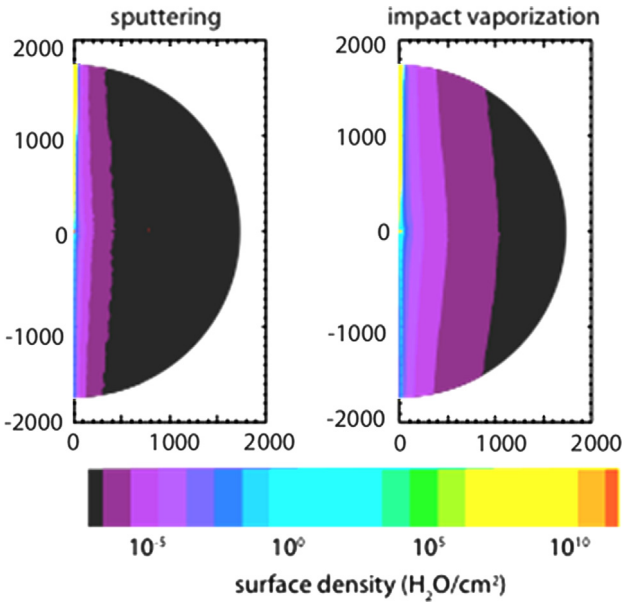

Fig. 2. Monte Carlo simulation of surficial water from a polar source emitting at a flux of $S \sim 10^{19}$ waters/s via sputtering and impact vaporization. Shown is a polar view of the surficial water over the dayside hemisphere. Note that water accumulates near the terminators.

Table 1
Results from Model #1 with 0.1 wt% icy regolith located at the floors of the polar craters.

	Yield (H_2O/event)	F (1/m^2-s)	$S=YFA_s$ (H_2Os/s)[d]
SW ion sputtering	10^{-3} [e]	2×10^{10}	2×10^{17} [f]
ESD	2×10^{-5} [a]	$<10^{12}$	$<10^{17}$
PSD cosmic Ly-α	2×10^{-6} [a]	10^{13}	2×10^{17}
Impact vaporization[b]	3×10^{14} [c]	$\sim10^{-7}$ [c]	3×10^{17} [b]

[a] Cross section from Thrower et al., 2010; Surface density ($n^{2/3}$) for 0.1 wt% icy regolith.
[b] Cintala, 1992, total vaporization at 10^{-16} g/cm^2-s; into regolith with 0.1 wt% water.
[c] Cintala, 1992, yield and flux for the 10^{-8} kg impactor; the peak in impactor vapor flux.
[d] Polar Cap Source Area$=10^{10}$ m^2.
[e] Weighted yield water from 0.1 wt% icy regolith.
[f] Spatially variable within a crater (Farrell et al., 2010), we apply solar wind flux value in central region of crater.

very small (~10^{-4}) along the flow-leading edge (leeward edge) inside the crater, and increases exponentially along the floor with distance from the obstacle edge. In the crater central regions, the ion inflow is F/F_{sw}~0.01 and at the far edge is F/F_{sw}~0.1. Thus, integrated over a lunation, floor regions located near crater walls will have a highly variable flux ratio, F/F_{sw}, from extreme low values of 10^{-4} to high values of 10^{-1} as the location moves from the leeward to far edge in the flow. Integrated over a lunation, the edges thus see F/F_{sw} a value slightly below 0.1. However, in the central regions of the craters, over a lunation, the ratio will have a quasi-constant value of F/F_{sw}~0.01 (see Fig. 2 of Jackson et al., 2011). The nominal diverted solar wind ion influx in the central floor region is thus approximated as F~2×10^{10}/m^2-s. As indicated in Table 1, over a crater floor source area of $A_s=10^{10}$ m^2, this provides S$\sim$YFA~2×10^{17} water molecules ejected per second. The result varies linearly with source area and ice concentration, and only applies to exposed icy-regolith (located within 100 Å of the surface).

The energy distribution of the sputtered polar water molecules varies as $1/E^2$ (Johnson, 1990) and thus will contain escaping molecules with velocities greater than the lunar escape speed. However, a fraction of lower energy molecules will return to the lunar surface, progressively covering the surface with water from mid-latitudes to the poles via the sputtering process.

3.2. Electron-stimulated and photon-stimulated desorption

In general, the yields for electron and photon stimulated desorption (ESD and PSD) are $Y_{esd}=P_e\sigma n^{2/3}$ where P_e is the incident energy going into ionization, σ is the specific interactions cross section, and $n^{2/3}$ is the substrate surface density (McGrath et al., 1986; Johnson, 1990). For ice abundances at 0.1 wt%, $n^{2/3}$ is ~10^{17}/m^2.

In the case of ESD, Thrower et al. (2010) found that $\sigma_{esd}=P_e\sigma$~10^{-22} m^2 making Y_{esd}~2×10^{-5} H_2Os per incident electron. Like the ions, the solar wind electron flux also flows into sheltered craters with a flux that is functionally similar to the ions, but increased by the ratio of electron thermal speed-to-ion flow speed (v_{te}/V~5). As such, the electron flux to the surface $\sim10^{11}$/m^2-s (Farrell et al., 2010; Zimmerman et al., 2011), making the ESD water source rate, S_{esd}~$Y_{esd}FA_s\sim2\times10^{16}$ H_2Os/s (see Table 1).

In the case of PSD, we consider the release of water via interaction with Lyman-α photons. Thrower et al. (2010) found that σ_{psd}~10^{-23} m^2 and for a surface density of molecules at ~10^{17}/m^2 corresponds to a yield Y_{psd}~2×10^{-6} waters/photon. The cosmic background Lyman-α flux is F~1×10^{13} photons/m^2-s (Gladstone et al., 2012) and thus makes the source rate S_{psd}~$Y_{psd}FA_s$~2×10^{17} H_2Os/s (see Table 1). The result for both electron and photon stimulated desorption varies linearly with source area, and only applies to exposed icy-regolith (ice has to be within a few Angstorms of the surface).

3.3. Impact vaporization

Impact vaporization is a potent mechanism for energizing and releasing material from the polar icy regolith. This process is attractive for two reasons: (1) the ice does not have to be directly exposed since the impact can penetrate below a dry cover layer and (2) an impact release at 4000 K has a nominal water velocity of ~2 km/s that will create a water scale height of 100's of kilometers and will have a lateral single hop distance of 100's of kilometers (i.e., capable of coating surfaces at lower latitudes). The micro-meteoroid impact vapor flux is found to be 10^{-15} kg/m^2-s (Cintala, 1992) and for a near-surface icy polar regolith with 0.1 wt% water provides an outward flux of Φ~3×10^7 H_2Os/m^2-s. When this flux is integrated over the crater area, we obtain $S_{impact}\sim\Phi A_s$~3×10^{17} H_2Os/s (Table 1).

As indicated in Table 1, integrated across all the processes, the polar source flux of water is no larger than 10^{18} H_2O's/s, with impact vaporization being the dominant source. Not every released molecule actually propagates to mid-latitude. In the case of ESD and PSD, the processes may be inherently low energy, leading to only local transport (condensation onto adjacent surfaces). Sputtering may be so energetic as to allow near complete ballistic escape into space. Impact vaporization may be an ideal process since it provides the proper energy to allow a substantial fraction of the released vapor to propagate to mid-latitudes.

4. Model 2: buried water within polar craters

Feldman et al., 1998 suggested that the hydrogen signature detected in the Lunar Prospector Neutron Spectrometer is best explained by an icy-regolith buried under many centimeters of a dry layer. Model 2 thus considers a 5 wt% icy regolith layer that is buried under a dry regolith. In this case, only impact vaporization can release the water since only this process can excavate deep into the regolith. Consider a buried 5 wt% icy-regolith layer at depth d. We will require the impactor to penetrate ~2d to excavate and vaporize a substantial volume of the buried ice layer. Integrating this ~2d penetration over the volume of both the dry and icy regolith, the amount of vapor is approximately 2 wt% of water. We assume simplistically that a little over half the vapor product is from the dry regolith and a little less than half is the 5 wt% icy regolith, giving rise to ~2 wt% water in the vapor. This is an approximation and does not take into account that water likely vaporizes at lower temperatures than the regolith, thus drawing larger water vapor products from the encasing icy-regolith. Our approach to determine the water vapor released: we first establish a layer depth, d, and water concentration. We then ask: what impactor could penetrate to 2d? The key relationship that allows analytical closure is the empirical scaling that crater depth, 2d, to impactor diameter, 2a, is d/a~9 (Gault, 1973). This relationship then allows us to estimate the associated impactor size and mass consistent with a 2d penetrator. Given an impactor's mass and a nominal impactor speed of 10 km/s at the Moon, we apply the scaling relationship in figure 5 of Cintala (1992) that the ejected vapor mass upon impact is approximately comparable to the impactor mass (for similar impactor/surface mass densities). Table 2 shows the resulting S rates for an ice layer 3, 20, and 50 cm depth, excavated by an impactor with mass of 4×10^{-4} kg, 0.1 kg, and 1.7 kg capable of penetrating to depth of 6, 40, and 100 cm respectively. Combining Gault (1973) and Cintala (1992) scaling relationships, the water yield per impact is derivable to form its

Table 2
Results from Model #2, assuming a 5 wt% icy-regolith layer buried at 3, 20, and 50 cm.

	Ice layer depth (cm)	Impactor depth (cm)	Yield (H_2O/impact event)	F (1/m^2-s)	$S=YFA_s$[c] (H_2Os/s)
Impact vaporization	3	6	2.4×10^{20} [a]	3×10^{-14} [b]	7×10^{16}
Impact vaporization	20	40	7×10^{22} [a]	3×10^{-17} [b]	2×10^{16}
Impact vaporization	50	100	1×10^{24} [a]	10^{-18} [b]	1×10^{16}

[a] Assuming an impact depth-to-diameter ratio=9 (Gault, 1973); $M_{vapor}\sim M_{impactor}$ (Cintala, 1992).
[b] Impact flux from figure 5 of Meyer-Vernet et al. (2009).
[c] Polar Cap Source Area=10^{10} m^2.

own scaling relationship as

$$Y^{water}_{impact} = CM_{vapor}/m_w \sim CM_{impactor}/m_w \sim C\rho_p 4a^3/m_w \quad (1)$$

where a is the impactor radius, C is the water vapor mass fraction integrated across the entire vapor product (i.e, ~2 wt%), ρ_p is the penetrator mass density, and m_w is the mass of a water molecule (~3.3×10^{-26} kg). These impact yields are listed in Table 2. Surprisingly, the overall water flux decreases relatively slowly with increasing layer depth. In essence, the reduction in frequency of impactors (Meyer-Vernet et al., 2009) is almost offset by the increased vapor yield per impact. The resulting water source rate from buried ice is a factor of at least 5 below that from the exposed ice case in Model 1.

We conclude that some water is always ejected to lower latitudes and thus accounts for a fraction of the OH veneer. Thus, we should expect some level of lunar polar water to be redistributed to mid-latitudes, even when the icy-regolith is buried.

5. Implications

A maximum source rate of S~10^{18} H_2Os/s amounts to $<10^{-7}$ kg/s of water to be ejected from each pole. Herein we assume each pole emits approximately the same amount of water. Neutron measurements suggest the H-bearing content at each pole has similar areal area (Feldman et al., 1998). However, shadowing studies suggest the North Pole may have a smaller collective region in shadow compared to the south and thus may possess less area of trapped water. The polar water fountain source rate is 10^{-5} lower than the overall exospheric source rate for all species (Stern, 1999). The primary water molecules are dynamic, being ejected from the poles and then undergoing ballistic 'hopping' trajectories to cooler regions (Crider and Vondrak, 2000). As such, these hopping water molecules will also contribute an added exospheric component. Given that the water photo-dissociation lifetime is $\tau_w\sim10^5$ s, the mass of water in the exosphere from the fountain and hopping components at any given time from both poles is approximately $2S\ \tau_w\ m_w$~0.02 kg, and this mass makes up 0.2 ppm of the total exosphere mass of ~100 t (Stern, 1999). As such, a polar water fountain source as described herein is a secondary exospheric process, and its contribution of a mid-latitude OH veneer is likely very subtle.

Given a total polar water source rate of 10^{18} H_2Os/s that is spread quasi-evenly over the mid-latitude region between 70–85° latitude (a band of 10^{12} m^2 in the each of the north and south), the incident mid-latitude water infall becomes F_w~10^6 H_2Os/m^2-s. On the nightside, this water would accumulate on the cold surface to levels of $F_w\times14$ days ~10^{12} H_2Os/m^2, to then undergo thermal desorption at sunrise. On the dayside, the water residency time is small (Crider and Vondrak, 2000) and surface-incident molecules begin to perform a random walk slowly migrating toward the cooler northern regions (see Fig. 1). However, the probability of photo-dissociation into OH along its return journey to the pole is close to unity. Following dissociation, the new OH molecule will be immediately adsorbed to the surface at mid-latitudes and will remain bound (the physioadsorbed molecule is considered 'sticky' with a desorption temperature of over 400 K (Hibbitts et al., 2011)). The OH molecule will remain on the surface until it undergoes photo-dissociation at time scales of τ ~10^7 s (Singh et al., 1983). In steady state, the water flux from an external source, F_w, has to equal the OH loss rate of N_{OH}/τ making the surface density of OH of N_{OH} ~10^{13}/m^2, with surface concentrations likely higher with latitude due to the quick migration of water at lower latitudes.

Can this water flux account for the 3 μm IR absorption feature reported by Pieters et al., 2009? As discussed in Dyar et al., 2010, for a monolayer of water on a flat surface, the IR reflectance would be minimal. However, for grainy/rough surfaces, there are larger IR absorption path lengths allowing a possible signal absorption. For a 1 μm grain, the cross-sectional area is A_g~3×10^{-12} m^2 and the number of OHs from a polar fountain source residing on this grain are then approximately $N_{OH}\ A_g$~30. This amounts to a molar fraction of water on the grain of ~10^{-8} which is too low for the M^3-inferred molar fraction of 6×10^{-3} (see note 21 of Pieters et al., 2009). The polar water flux is apparently too low to account for the M^3 observations of the mid-latitude water veneer, but it is still anticipated this source provides some contribution at mid-latitudes from a polar outflow. The model also predicts a local exosphere of water directly over polar crater source regions like Shoemaker and Cabeus with an upward flux of S/A_s~10^8/m^2-s.

Fig. 2 shows a result of a Monte Carlo simulation of water molecules ejected from the poles at a flux of 10^{19} water/s for a sputtered and impact vaporization polar fountain source. The model (Crider and Vondrak, 2000) includes residency time and thermal migration of water from a polar fountain source as it interacts with the surface. The sputtered-driven water molecules shown in the left hand side have limited latitudinal dayside concentration because a larger relative fraction is ejected at speeds exceeding the gravitational escape speed. In contrast, impact vaporized polar water provides a veneer at mid-latitudes, albeit at very low concentrations. Once landing at mid-latitudes, the water immediately initiates its migration back toward the pole via a thermal diffusion process with the surface. The water residency time is short on the warm dayside surface. For example, using the mid-latitude water infall value derived above at F_w~10^6 H_2Os/m^2-s and a water surface residency time of 0.5 μs then the instantaneous water surface veneer has a value of ~1 H_2Os/m^2 (or 10^{-4}/cm^2) similar to the shaded purple/blue regions in Fig. 2. At the terminator and poles, the water surface residency time is longer, and surface concentrations thus increase at these cooler locations. The spatial distribution of the water appears similar to observation, but the overall values are substantially reduced from observation (Pieters et al., 2009).

The results in Fig. 2 are scalable with water fountain source S. As such the veneer is even weaker when considering the polar fountain created from buried water in polar craters (Table 2). In this case, $S<10^{17}$ H_2Os/s, and the surface concentrations/veneer associated with impact vaporization should have a similar spatial distribution but an overall flux level reduced by 1/100th of the values shown in the color bar of Fig. 2.

At a global level, this model predicts the presence of two flows for the water: (1) An energetic flow from the poles as ejected

molecules travel toward the equator at high altitudes (few hundred kilometers) with high speeds consistent with impact vaporization. About ½ of the distribution may actually fully escape from the Moon. (2) A low energy/low altitude poleward flow associated with the thermally migrating population (Butler, 1997; Crider and Vondrak, 2000). This poleward flow will be less energetic and most molecules will photo-dissociate before returning to their source. Thus, there is a bi-directional flow at mid-latitudes, but stratified in height. It is interesting to consider the idea that some fraction of the water molecules (~4%) may return all the way back to its parent pole (Crider and Vondrak, 2000), only to be ejected once again via a second impact vaporization event. An even smaller fraction of water molecules may have undergone multiple ejections and returns.

We have assumed that there is a source of water within polar craters and the process described herein represents an obvious loss process to that localized source. We judiciously do not address the original source of the water in polar craters themselves. However, it has been demonstrated that comet and asteroid impacts at the Moon can be an impulsive source of water that could be retained at the poles at levels 10^8 to 10^9 metric tons when integrated over a billion years (Ong et al., 2010). The compositional diversity found in the LCROSS plume from the floor of Cabeus crater provides some supporting evidence for an extra-lunar source (Colaprete et al., 2010; Schultz et al., 2010). However, that conclusion is not unique. The environmental loss processes described herein (impact vaporization and sputtering) represent a loss rate of no more than 10^{-7} kg/s or a loss of surficial water mass of ~4×10^6 metric tons over 1 Gyr. However, these rates are a function of the surficial water content itself, where 0.1 wt% of water has been assumed. If the regolith water content for periods closely following impact lie closer to 10%, the rates in Table 1 also increase by a factor of 100 to values closer to 10^8 t/Gyr. In other words, the environment extracts water from the polar crater surface, but not by thermal processes like sublimation—instead relying on more violent processes like impact vaporization and sputtering to self-provide the required heat/energy for molecular transport. Over time, these top layers in polar craters effectively 'dry out' as they are space weathered, gardened, and buried (Hurley et al., 2012).

The upcoming Lunar Atmosphere and Dust Environment Explorer (LADEE) mission provides a unique opportunity for further constraining this model (and others) regarding lunar polar water. In this case, the UVS could search for the high altitude polar outflow of water molecules (i.e., H_2O^+ near a wavelength of ~610 nm) that would be expected from polar weathering. UVS can also detect OH and OH^+ allowing it to behave as an exospheric water detector (Colaprete et al., 2010).

6. Conclusions

The calculations above describe a quasi-steady state situation that includes the near steady micro-meteoroid stream onto the polar crater floors. However, on rare occasions, a larger impactor may occur that impulsively releases a larger concentration of water from the crater floor. Using Eq. (1), if a 100-kg object impacted a polar crater floor, assuming a 2% buried icy-regolith, the water yield would be near 10^{26} water molecules released in an impulsive burst that would be added to the quasi-continual fountain emitting near 10^{18} water molecules/s. Such an event might occur on a scale of 10's of years. These impulsively-released water molecules would migrate from the dayside to the terminator over the course of a few days (Crider and Vondrak, 2000). In essence, the terminator and nightside regions would have enhanced concentrations of water that would get continually re-released as these regions rotated into dawn. As such, we would expect the dawn terminator to be an active site for water desorption over many lunations after the polar crater impact. Reemission will occur until complete water photo-dissociation into OH occurs. This terminator-released newly-minted OH may then reside on the surface for 100's of days due to its relatively high desorption temperature (Hibbitts et al., 2011) until it also is lost to photo-dissociation (OH photo-dissociation times is ~10^7 s (Singh et al., 1983)) or other environmental processes like sputtering or impacts. Hence, given a large impact into the polar crater water-rich region and an enhanced impulsive polar water fountain, we suggest there could be the development of a second water-OH cycle occurring along the dawn terminator over many lunations after the impact.

As described above, at mid-latitudes, in a quasi-steady situation, the polar water source (S~10^{18} waters/s) raining onto the surface has to ultimately balance against OH photo-dissociative losses, yielding a value of surfical OH of N_{OH} ~10^{13}/m^2. We assume that this OH is spread homogenously over all dust grains (to yield 30 OH's per each 1 μm grain). However, it may be that the OHs sequester in shadowed or protected regions on the surface. In these shadowed regions (like at the base of a dust grain, local depressions, etc.) OH may build up to higher levels over time. To what extent this effect occurs requires a separate rough surface illumination and thermal model. While it remains unclear if such a build-up accounts for the M^3 observations, we can only say that we have assumed a homogenous spread of OH over a surface in these calculations, which is a highly-idealized assumption. Rough surfaces may provide local heterogeneous regions of enhanced OH concentration.

To summarize, this polar water 'fountain' model suggests that there should be an outflow of polar water from cold trap regions to mid-latitudes, with cold-trapped water energized by impacts and solar wind. While the predicted polar migration may not fully account for the relatively high concentrations in the mid-latitude water veneer observed in the IR (at an abundance 10–1000 ppm), it may account for some small part of the veneer. Taking the conservative case that polar water is ejected only from the floor of polar craters with an 0.1% icy regolith then overall source rates are no more than $\sim 10^{18}$ H_2Os/s. However, the source rates scale linearly with concentration, and larger mass fractions of polar water provide correspondingly larger fractions of water emission out of the poles.

References

Arnold, J.R., 1979. Ice in the lunar polar regions. Journal of Geophysical Research 84, 5659–5668.

Butler, B.J., 1997. The migration of volatiles on the surfaces of Mercury and the Moon. Journal of Geophysical Research 102, 19283.

Cintala, M.J., 1992. Impact-induced thermal effects in the lunar and Mercurian regliths. Journal of Geophysical Research 97, 947.

Clark, R.N., et al., 2009. Detection of adsorbed water and hydroxyl on the Moon. Science 326, 562.

Colaprete, A., et al., 2010. Detection of water in the LCROSS ejecta plume. Science 330, 463.

Crider, D.H., Vondrak, R.R., 2000. The solar wind as a possible source of lunar polar hydrogen deposits. Journal of Geophysical Research 105, 26773.

Dyar, M.D., Hibbitts, C.A., Orlando, T.M., 2010. Mechanisms for incorporation of hydrogen in and on terrestrial planetary surfaces. Icarus 208, 425.

Farrell, W.M., et al., 2010. Anticipated electrical environment within permanently shadowed lunar craters. Journal of Geophysical Research 115, E03004.

Feldman, W.C., et al., 1998. Fluxes of fast and epithermal neutrons from Lunar Prospector: Evidence for water ice at the lunar poles. Science 281, 1496.

Gault, D.E., 1973. Displaced mass, depth, diameter, and effects of oblique trajectories for impact craters formed in the dense crystalline rocks. The Moon 6, 32.

Gladstone, G.R., et al., 2012. Far-ultraviolet reflectance properties of the Moon's permanently shadowed regions. Journal of Geophysical Research 117, E00H04.

Hibbitts, C.A., et al., 2011. Thermal stability of water and hydroxyl on the surface of the Moon from temperature-programmed desorption measurements of lunar analog materials. Icarus 213, 64.

Housley, R.M., et al., 1974. Solar wind and micrometeorite alteration of the lunar regolith. In: Proceeding of the Fifth Lunar Conference, Geochimica et Cosmochimica Acta 3 (Suppl. 5), pp. 2623–2642.

Hurley, D.M.,, et al., 2012. Two-dimensional distribution of volatiles in the lunar regolith from space weathering simulations, Geophys. Res. Lett. 39, L09203, http://dx.doi.org/10.1029/2012GL051105.
Jackson, T.L., et al., 2011. Discharge of roving objects in the lunar polar regions. Journal of Spacecraft and Rockets 48 (4), 700–703.
Johnson, R.E., 1990. Energetic Charged Particle Interactions With Atmospheres and Surface. Spinger, New York.
Lanzerotti, L.J., Brown, W.L., Johnson, R.E., 1981. Ice in the polar regions of the Moon. Journal of Geophysical Research 86, 3949–3950.
McCord, T.B., Taylor, L.A., Combe, J.P., Kramer, G., Pieters, C.M., Sunshine, J.M., Clark, R.N., 2011. Sources and physical processes responsible for OH/H_2O in the lunar soil as revealed by the Moon Mineralogy Mapper (M3). Journal of Geophysical Research 116, E00G05.
McGrath, M.A., Johnson, R.E., Lanzerotti, L.J., 1986. Sputtering of sodium on the planet Mercury. Nature 323, 694.
Meyer-Vernet, N., et al., 2009. Dust detection by the Wave instrument on STEREO: nanoparticles picked up by the solar wind. Solar Phys 256, 463, http://dx.doi.org/10.1007/s11207-009-9349-2.
Mitrofanov, I.G., et al., 2010. Hydrogen mapping of the lunar south pole using the LRO neutron detector experiment LEND. Science 330, 483.
McCord, T.B., et al., 2011. Sources and physical processes responsible for the OH/H_2O in the lunar soil as revealed by the Moon Mineralogy Mapper (M3). Journal of Geophysical Research 116, E00G05.
Morgan, T.H., Shemansky, D.E., 1991. Limits to the lunar atmosphere. Journal of Geophysical Research 96, 1351–1367.
Ong, L., et al., 2010. Volatile retention from cometary impacts on the Moon. Icarus 207, 578–589.
Pieters, C.M., et al., 2009. Character and spatial distribution of OH/H_2O on the surfaceof the Moon seen by M3 on Chandrayaan-1. Science 326, 568.
Schultz, P.H., et al., 2010. The LCROSS cratering experiment. Science 330, 468.
Singh, P.D., et al., 1983. The photodissociation lifetimes of the OH and OD radicals in comets. Icarus 56, 184–189.
Stern, S.A., 1999. The lunar atmosphere: history, status, current problems and context. Reviews of Geophysics 37, 453.
Sunshine, J.M., et al., 2009. Temporal and spatial variability of lunar hydration as observed by the Deep Impact spacecraft. Science 326, 565.
Thrower, J.D., et al., 2010. Photon and electron stimulated desorption from laboratory models of interstellar ice grains. Journal of Vaccum Science and Technology A 28, 799.
Zimmerman, M.I., Farrell, W.M., Stubbs, T.J., Halekas, J.S., Jackson, T.L., 2011. Solar wind access to lunar polar craters: feedback between surface charging and plasma expansion. Geophysical Research Letters 38, L19202, http://dx.doi.org/10.1029/2011GL048880.